Available online at www.sciencedirect.com

ScienceDirect

Ceramics International 40 (2014) 2557–2564

CERAMICS INTERNATIONAL

www.elsevier.com/locate/ceramint

Review paper

Improved mechanical properties of SnO_2:F thin film by structural modification

Qian Gao[a], Hong Jiang[b,*], Ming Li[a], Peng Lu[c], Xinyu Lai[c], Xiang Li[a], Yong Liu[a], Chenlu Song[a], Gaorong Han[a,*]

[a]*State Key Laboratory for Silicon Materials and Center for Electron Microscopy, Department of Materials Science and Engineering, Zhejiang University, Hangzhou 310027, China*

[b]*Special Glass Key Laboratory of Hainan Province, Hainan University, Hainan 570228, China*

[c]*Aviation Industry Corporation of China (HAINAN) Special Glass Material CO., LTD; Special Glass Engineering Technology Research Center of Hainan Province, Hainan 570228, China*

Received 14 June 2013; received in revised form 29 July 2013; accepted 18 August 2013
Available online 4 September 2013

Abstract

This study reports the improvement in the mechanical properties of SnO_2:F (FTO) thin films through the modification of the structure and surface morphology. The FTO thin films are deposited on glass substrates by the atmospheric pressure chemical vapor deposition method on an industrial production line. Both the average grain size and the surface roughness were progressively increased by increasing the flow rate of metal organic monobutyltin trichloride (MBTC). The hardness and Young's modulus of the FTO films increased from 9.01 GPa to 15.08 GPa, and from 125.24 GPa to 206.93 GPa, respectively, according to the nanoindenter results. Post-heat treatment at 650 °C for 10 min resulted in a further increase in the hardness and Young's modulus, reaching maximum values of ~15.89 GPa and ~235.9 GPa, respectively. The enhancement in mechanical properties can be attributed to the reduced grain boundaries and the improved structural densification.

Keywords: Fluorine-doped tin oxide; Flow rate; Post-heat treatment; Mechanical properties

Contents

1. Introduction

Transparent conducting oxide (TCO) films, which have outstanding optical transparency (more than 80%) in the visible spectrum range and high electrical conductivity (~$10^3\ \Omega^{-1}\ cm^{-1}$ or more), have been widely used in optoelectronic applications

*Correspondence to: State Key Laboratory for Silicon Materials and Center for Electron Microscopy, Department of Materials Science and Engineering, Zhejiang University, Hangzhou 310027, China. Tel.: +86 571 87951649; fax: +86 571 87952341.
E-mail address: hgr@zju.edu.cn (G. Han).

0272-8842/$ - see front matter © 2013 Elsevier Ltd and Techna Group S.r.l. All rights reserved.
http://dx.doi.org/10.1016/j.ceramint.2013.08.082

such as solar cells and displays. Typical TCO materials include indium tin oxide (ITO), aluminium-doped zinc oxide (AZO), boron-doped zinc oxide (BZO) and fluorinated tin oxide (SnO_2:F, FTO) [1–4]. However, due to the poor thermal stability and high cost of ITO films, inexpensive and non-toxic tin oxide films have attracted worldwide attention as potential alternatives [5,6]. The most widely used method for the industrial preparation of FTO films is chemical vapor deposition (CVD), due to its low cost, efficient film growth and good process stability.

In addition to monitoring the electrical and optical properties by carefully controlling the processing parameters, successful fabrication of FTO thin film-based devices requires a better understanding of the mechanical characteristics of the films, as the contact loading during processing or packaging can significantly worsen the device performance [7]. Therefore, there is growing interest in investigations of the mechanical characteristics of FTO thin films, in particular at the nanoscale regime. Nanoindentation is currently the most prominent technique to investigate and characterize the mechanical properties of materials at the sub-micron scale. This technique has been widely used to study the elastic–plastic and fracture properties on the surfaces of bulk samples as well as thin films [8,9]. Among the various mechanical properties of these films, the Young's modulus and hardness are of the greatest interest, as they reflect the elastic deformation and resistance to permanent deformation. The optical and electrical properties of tin oxide films have recently been investigated [10–12]. However, the mechanical properties of tin oxide films are rarely studied, and particularly little is known about the dependence of those properties on the microstructure.

This study therefore focuses on improving the mechanical properties of FTO thin films deposited via the atmospheric pressure chemical vapor deposition (APCVD) method on an industrial production line. The modification of the structure and surface morphology will be investigated. A series of FTO thin films were prepared, and the dependence of their mechanical properties on crystalline structure, grain size and surface morphology will be discussed.

2. Experimental methods

The SnO_2:F thin film was deposited on a soda lime glass substrate (thickness of 2 mm) coated with a $Sn_xSi_yO_2$ barrier by the APCVD method on an industrial production line as illustrated in Fig. 1. The temperature of the glass surface was maintained at ~690 °C, and the glass ribbon was drawn at a speed of 11.55 m/min with a 13 s deposition time. The main purpose of the barrier layer is to restrict the diffusion of alkali metal ions from the hot glass substrate into the SnO_2:F functional layer [13]. Metal organic monobutyltin trichloride (MBTC, $C_4H_9SnCl_3$, 99.0 wt%, Atofina Chemicals Co., Ltd.), tetraethoxysilane (TEOS, $C_8H_{20}O_4Si$, 99.0 wt%, Atofina Chemicals Co., Ltd.) and trifluoro acetic acid (TFA, CF_3COOH, 99.0 wt%, Jinhua Huasen Chemicals Co., Ltd.) were used as precursors for the $Sn_xSi_yO_2$ barrier layer. The flow rates were set at 15 kg/h for MBTC, 8 kg/h for TEOS and 4 kg/h for TFA. Only MBTC and TFA were used as precursors for the SnO_2:F layer. To modify the structure of the FTO thin films, different MBTC flow rates were used of 100 kg/h, 200 kg/h and 300 kg/h. The corresponding flow rates of TFA were 16 kg/h, 12 kg/h and 8 kg/h, respectively. In a previous study we reported that the variation of TFA content in the precursor controls the electrical property of the material by varying the fluorine doping concentration without modifying the structure [14]. Highly uniform FTO thin films with an average sheet resistance of ~11 Ω sq^{-1} and a resistivity of 10^{-4} Ω cm can be produced. High optical transmittance values of ~80% have also been observed for FTO coated glass [14]. These FTO thin films exhibited sufficient optical transparency and electrical conductivity for use in solar cells or other applications. The as-deposited glass was post-heated in air at 650 °C for 10 min.

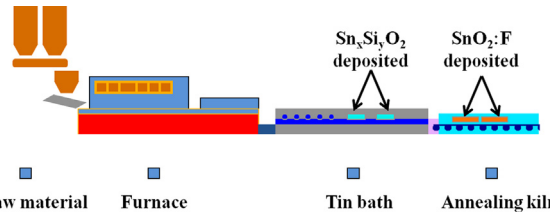

Fig. 1. A schematic diagram of the industrial production line for SnO_2:F/SiC_xO_y coated low-e glass.

The crystalline phase of the prepared films was determined by a D/max-RA X-ray diffraction instrument (XRD, Thermo electron ARL X'TRA) with 2θ values ranging from 20° to 70°. Comparison with JCPDS data shows that the films were preferentially oriented along the (200) direction, and other orientations were observed with very low intensities. The prominence of the (hkl) orientation was expressed in terms of the parameter 'relative prominence' [RP(hkl)], defined as

$$RP(hkl) = I_{hkl}/\sum(I_{hkl})(\%) \quad (1)$$

where I_{hkl} is the intensity of the (hkl) Bragg reflection [15]. The film surface morphology and root-mean-square (RMS) roughness were examined using a scanning electron microscope (SEM, SU-70, Hitachi) and atomic force microscope (AFM, Veeco, Dimension® EdgeTM). The nanomechanical properties were examined by nano-indentation (Agilent G200, USA) using the continuous stiffness measurement (CSM) technique.

In the nano-indentation experiment, a sharp and rigid Berkovich diamond indenter (three-faced indenter-tip) was continuously driven into the film by applying a loading force. The loading force and the corresponding indentation depth (displacement) of the indenter into the film surface were continuously recorded to generate the load–displacement curve. The load–displacement curve shows the response of the material to deformation under a perpendicular stress, which is used to determine the elastic modulus and hardness on the surface of the film. In principle, the traditional mechanical parameters of a material such as Young's modulus (E) and hardness (H) can be calculated using the following equations proposed by Oliver and Pharr [16,17]:

$$\frac{E}{1-\nu^2} = \frac{\sqrt{\pi}}{2}\frac{1}{\sqrt{A_{max}}}\frac{dP}{dh} \quad (2)$$

and

$$H = \frac{P_{max}}{A_{max}} \quad (3)$$

where dP/dh is the slope of the indentation unloading curve at the maximum load, P_{max} is the maximum applied load, A_{max} is the maximum contact area under the maximum load and ν is the Poisson's ratio of the specimen. FTO is considered to be a normal ceramic material, and the ν of FTO is set to 0.25 in this study [7]. To determine the values of the Young's modulus and hardness of the FTO films, a suitable range of indentation penetration depths was tested. The nano-indentation results are strongly affected by the properties of the substrates. To avoid the substrate effect, the indentation depth must be less than one-tenth of the film thickness [18].

3. Results and discussion

3.1. Structure and morphology of the FTO films

All films prepared in this work exhibited a polycrystalline rutile structure consistent with the characteristics of the SnO_2 structure (P42/mnm (136)) in JCPDS card 41-1445 (Fig. 2a). These films were highly oriented along the (200) direction. Other orientations were observed, including (110), (101), (211), (220), (310), (301) and (400), but these were less dominant. No peaks from impurities such as fluorine were detected at the resolution of this instrument. As the flow rate of MBTC increased, corresponding diffraction peaks became sharper and stronger, especially the (200) peak, indicating that the crystallinity of the films was improved. Fig. 2(b)–(d)

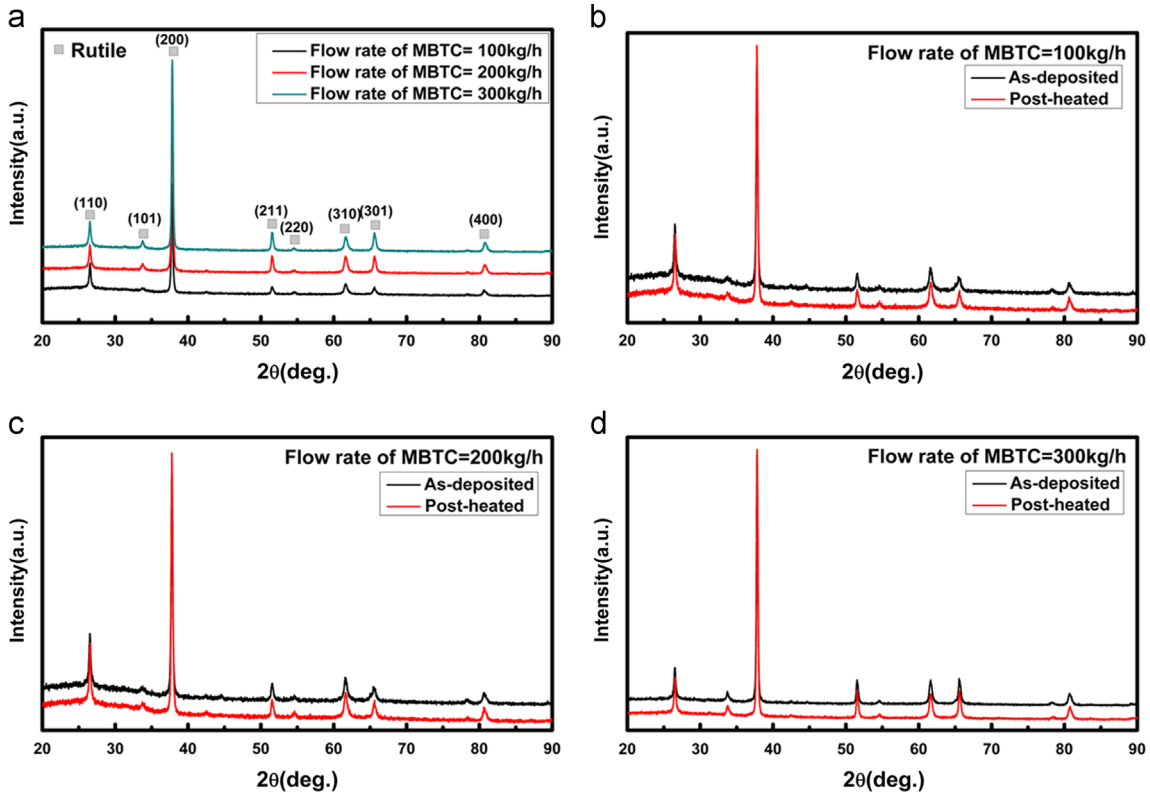

Fig. 2. (a) XRD patterns of as-deposited FTO thin films prepared with different flow rates of MBTC, and (b)–(d) the comparison of the XRD patterns between the as-deposited and post-heated FTO thin films.

Table 1
The *RP*(*hkl*) values of the as-deposited and post-heated FTO thin films with different flow rates of MBTC.

***RP*(*hkl*)/%**	**(110)**	**(101)**	**(200)**	**(211)**	**(220)**	**(310)**	**(301)**	**(400)**
100 kg/h MBTC, as-deposited	13.0	1.3	65.7	4.6	1.5	6.7	4.1	3.0
100 kg/h MBTC, post-heated	13.1	1.1	67.9	4.2	1.3	5.4	3.6	3.4
200 kg/h MBTC, as-deposited	8.4	2.0	66.5	7.0	7.5	5.5	6.9	3.0
200 kg/h MBTC, post-heated	7.4	2.3	67.8	6.2	0.7	5.5	7.1	3.1
300 kg/h MBTC, as-deposited	7.0	1.8	70.0	6.1	0.7	5.1	5.8	3.2
300 kg/h MBTC, post-heated	7.4	1.7	71.4	4.9	0.7	5.5	5.1	3.3

compare the XRD patterns between the as-deposited and the corresponding post-heated FTO thin films. The increased intensity of the diffraction peaks confirms the progressive modification of the structure by post-heat treatment. The enhancement of the crystallinity of similar FTO and ITO thin films by post-heat treatment has also been reported elsewhere [19,20]. Table 1 shows the *RP*(*hkl*) values of the eight orientations for the as-deposited and post-heated FTO films. According to these values, the as-deposited and post-heated FTO films preferentially oriented along the (200) direction. The increased flow rate led to an enhanced oriented growth along the (200) direction. The growth rate-dependent evolution of the orientation has been discussed. The previous work on un-doped spray-deposited SnO_2 films of Agashe et al. [21] showed that precursor concentration is the most important process parameter controlling growth rate and structural properties, which thereby determine the electrical properties. Results given by Belanger et al. [22] for SnO_2-based films deposited by chemical vapor deposition demonstrated that the dominant (200) direction could arise from a higher growth rate due to a higher precursor concentration. Another study reported that the texture along the (200) orientation can lead to an optimized balance between the electrical resistivity and the optical transmittance [23]. Therefore, the improved preferential orientation in the (200) direction is beneficial to the properties of SnO_2:F thin films.

The surface morphology and thickness of TCO films are important factors for their optical, electrical and mechanical properties. All of the films prepared in this work exhibited a fairly uniform surface morphology (Fig. 3(a)–(c)). The grain size increased from ~200 nm to ~400 nm as the flow rate of MBTC increased. Furthermore, the corresponding film thickness was found to increase from ~450 nm to ~870 nm, with a typical columnar growth structure (Fig. 3(d)–(f)). These findings indicate that higher flow rates of MBTC modify the structure of the resulting material by accelerating the growth rate and increasing the degree of grain agglomeration. The film surface morphology exhibited little variation under post-heat treatment as observed by SEM, which is expected due to the high degree of grain agglomeration and crystallinity of these FTO thin films, in good agreement with our previous work [24].

The two-dimensional surface morphology and three-dimensional depth profiles of the as-deposited and post-heated FTO thin films were revealed using AFM, as shown in Fig. 4. A remarkable evolution in the film morphology was observed, with small grains aggregating into large grains as the flow rate increased or following heat treatment, matching well with the SEM results. During the film deposition, in addition to the normal grain growth, a process of abnormal grain growth occurred at the surface of the thickening film. Briefly, smaller primary grains were consumed by larger secondary grains growing due to atomic diffusion, facilitating the repair of the dislocated atomic occupancies and promoting the coalescence of adjacent grains [25,26]. In our case, higher flow rates and heat treatment induced the process of abnormal grain growth due to the presence of more energy available to activate atomic diffusion. As measured from Fig. 4, the root-mean-square (RMS) values of the surface roughness increase from 14.5 nm, 22.1 nm and 29.4 nm for the as-deposited FTO as the flow rate of MBTC increases. The corresponding RMS values for the post-heated films are 15.9 nm, 23.3 nm and 30.7 nm, respectively. The light scattering ability of a rough surface is well known to be determined by the feature size and shape of the grains in the thin films. Thus, the light trapping ability of the FTO film was improved by the modification of the film structure and surface.

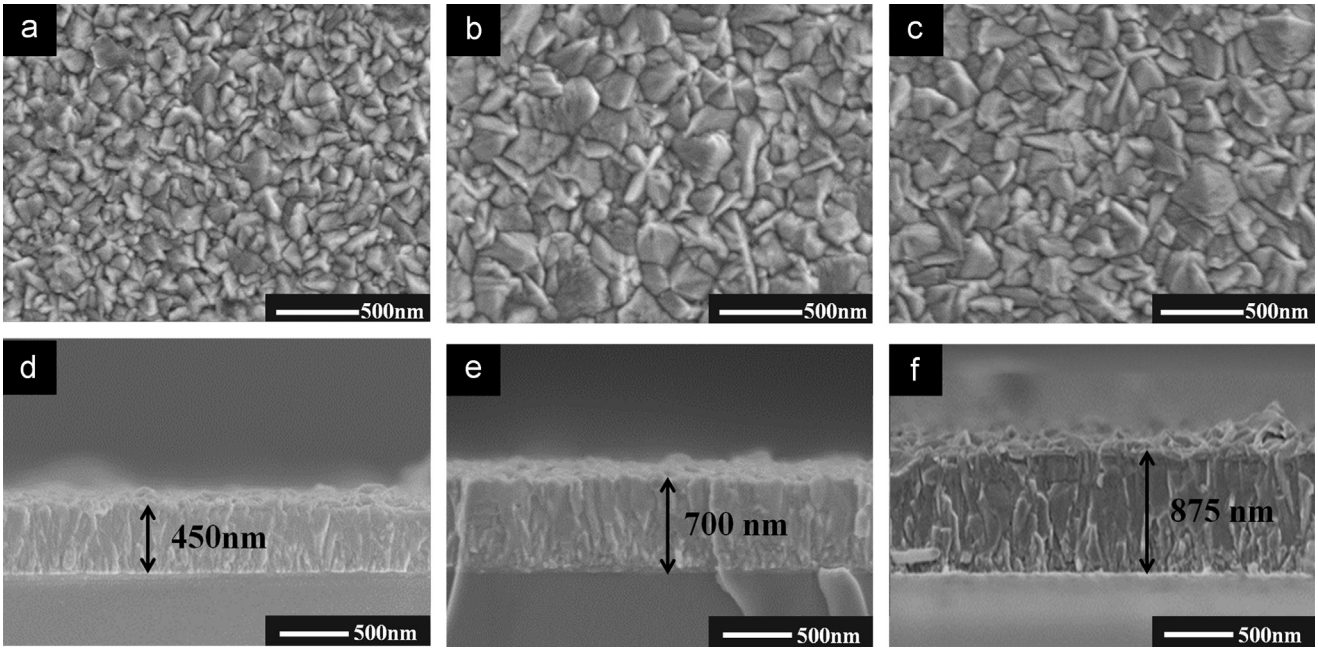

Fig. 3. SEM micrographs of the FTO films deposited with various flow rates of MBTC: (a) 100 kg/h, (b) 200 kg/h, (c) 300 kg/h; and (d)–(f) cross-sectional micrographs of the corresponding films.

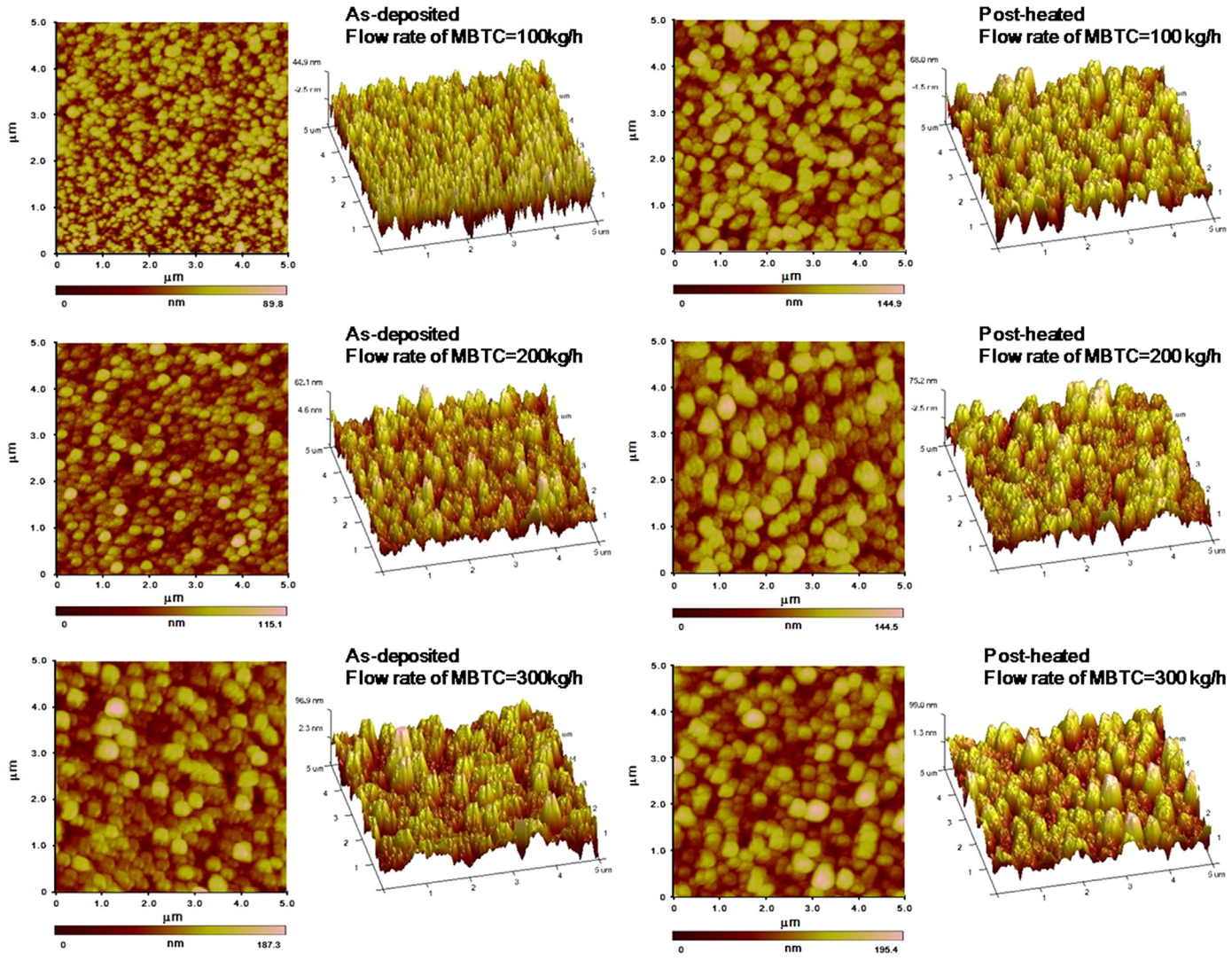

Fig. 4. AFM images of as-deposited and post-heated FTO thin films with different flow rates of MBTC.

3.2. Mechanical properties of the FTO films

Reliable mechanical properties are vital to ensure good and stable device performance. The indentation load–displacement curves of the as-deposited and post-heated FTO thin films are shown in Fig. 5. The area between the loading and unloading curves represents the plastic deformation energy. The area below the unloading curve represents the elastic deformation energy. The entire area below the loading curve is the total deformation energy. The load-displacement curves of all as-deposited or post-heated films exhibit the typical indentation behavior of oxide ceramic materials. The degree of elastic recovery is defined as $R=(d_{max}-d_{res})/d_{max}$, where d_{max} and d_{res} represent the displacement at the maximum load and the residual displacement after unloading, respectively [27]. As calculated from the load–displacement curves in Fig. 5 (a), the elastic recovery of the as-deposited films was ~45%, significantly higher than that of the metal films. In addition, as shown in Fig. 5(b)–(d), the comparison between the load–displacement curves of the as-deposited and post-heated FTO thin films demonstrates that the plastic deformation energy increased in each post-heated film.

The hardness and Young's modulus of the as-deposited and post-heated FTO films were calculated from the load–displacement data following the Eqs. (1) and (2). The calculated hardness–displacement and Young's modulus–displacement curves of the three films prepared under different flow rates exhibited similar trends. The hardness and Young's modulus of the FTO film prepared at an MBTC flow rate of 100 kg/h are shown in Fig. 6. Both the hardness–displacement plots can be divided into two stages, with initial growth occurring as displacement is increased, followed by the establishment of a constant value. The increase in hardness at low penetration depths is usually attributed to the transition from purely elastic to elastic/plastic contact. At this stage, the hardness is not accurately measured by the mean contact pressure. The mean contact hardness only represents the hardness under the condition of a fully developed plastic zone [16]. After the first stage, the hardness reached a constant value consistent with that of a monolithic material. Therefore, the hardness

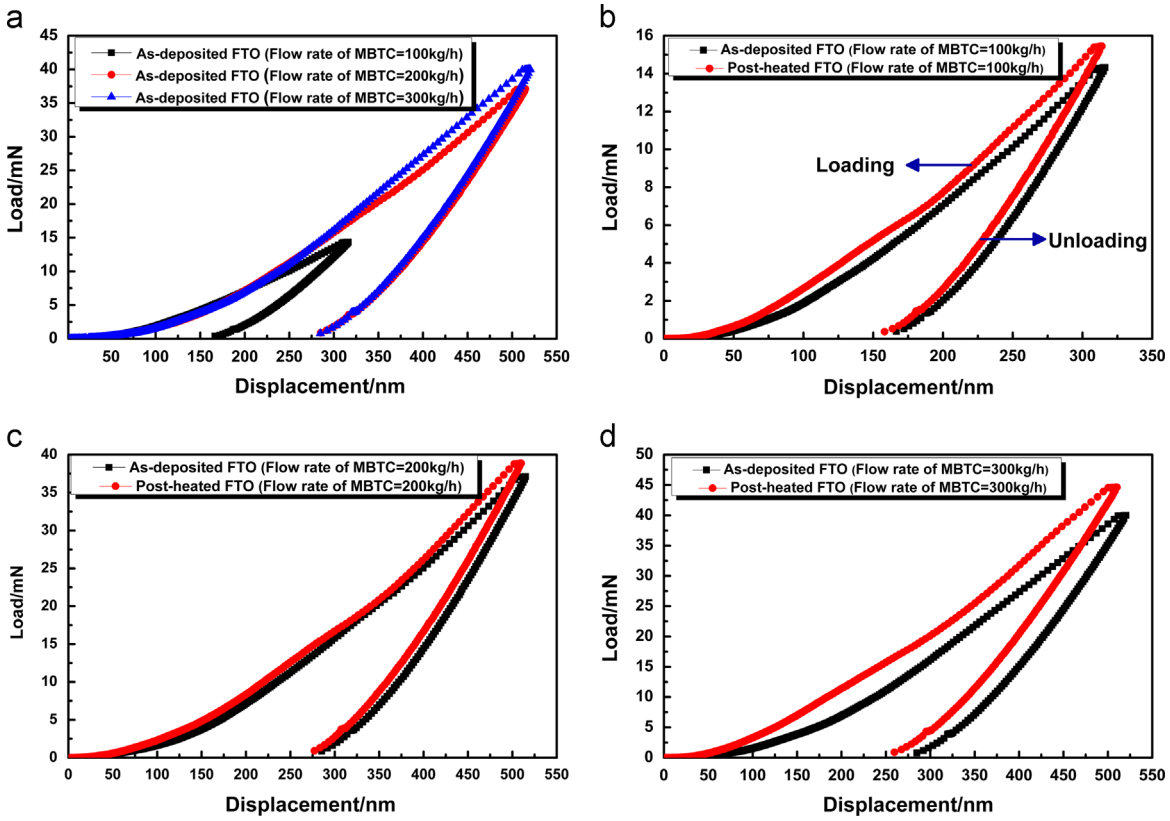

Fig. 5. Typical load-displacement curves of as-deposited and post-heated FTO thin films with different flow rate of MBTC.

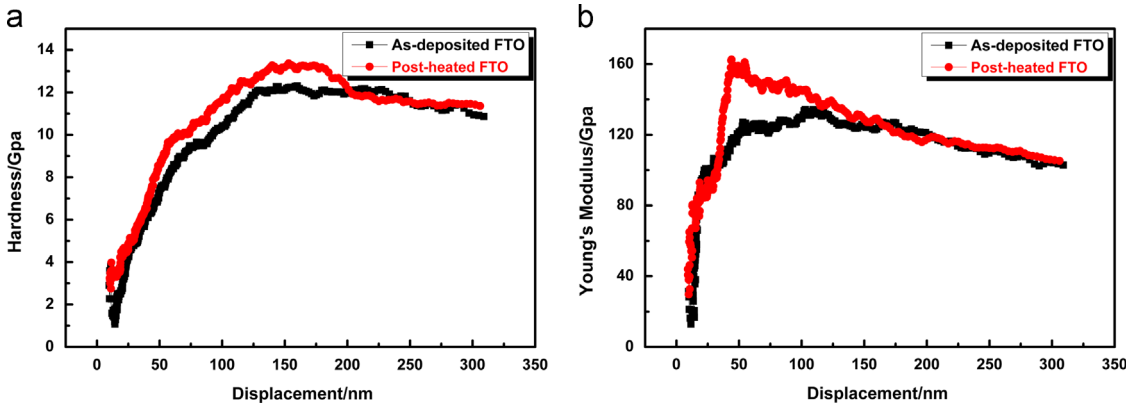

Fig. 6. Nanoindentation results: (a) the hardness–displacement and (b) Young's modulus–displacement curves of as-deposited and post-heated FTO thin films with an MBTC flow rate of 100 kg/h.

values at this stage were regarded as intrinsic properties of the films. The variation in the Young's modulus follows a similar pattern as the hardness. The results indicate that a range exists over which the intrinsic Young's modulus and hardness can be determined and the influence of the substrate can be ignored. For films deposited with thicknesses of ~500 nm, this region was an indentation depth of ~120–170 nm. The same regions for thin films with thicknesses of ~700 nm and ~900 nm were ~120–190 nm and ~120–210 nm, respectively.

As demonstrated in Fig. 3, the grain sizes of FTO films prepared with increasing flow rates are ~200 nm, ~300 nm and ~400 nm, respectively. To determine the effect of the evolution of the surface microstructure on the mechanical properties of the film, the relationship between the average grain size and the Young's modulus and hardness values of the FTO films were plotted (Fig. 7). The Young's modulus and hardness of the as-deposited FTO films increased from 125.24 GPa to 206.93 GPa and from 9.01 GPa to 15.08 GPa, respectively, as the average grain size increased. Furthermore, the Young's modulus and hardness increased after post-heat treatment. The maximum values were ~235.9 GPa and ~15.89 GPa, respectively, which were observed for the post-heated FTO thin film with a grain size of ~400 nm. The highest Young's modulus of the SnO_2:F thin film

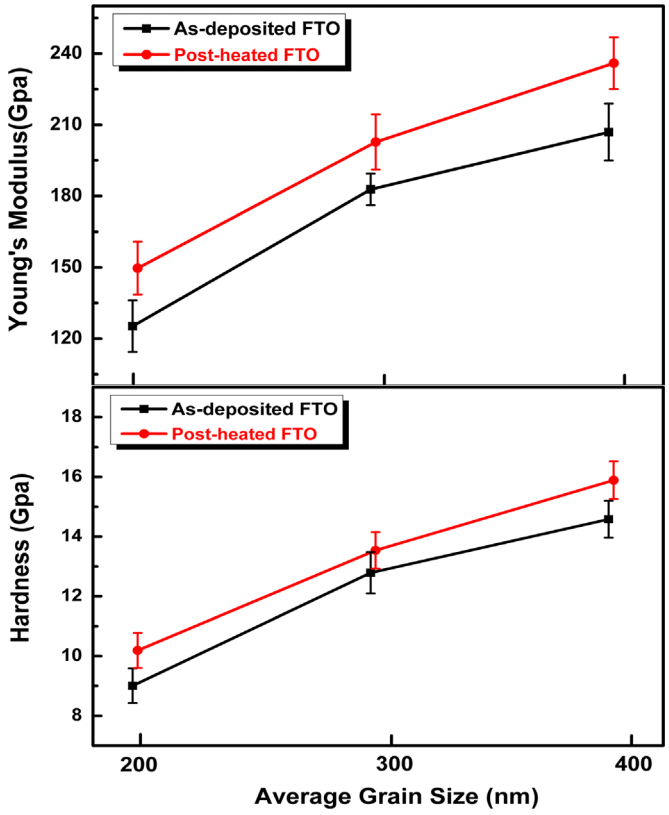

Fig. 7. The average Young's modulus and hardness of the as-deposited and post-heated FTO thin films as a function of increasing average grain size.

deposited by chemical vapor deposition on a glass substrate was recently reported to be less than 100 GPa [28]. In addition, the highest hardness value documented for the SnO_2:F thin films is less than 10 GPa. For other TCOs, the Young's modulus of ITO and AZO films deposited by various methods have been reported to be below 150 GPa [29,30]. The hardness values of SnO_2:Sb and ITO thin films deposited via sputtering have been reported to be ~21.7 GPa and ~17.5 GPa, respectively [31]. TCO thin films deposited via sputtering exhibited better mechanical properties, including hardness, but this study also improved the mechanical properties of SnO_2:F thin films by modifying the structure by increasing the flow rate and performing post-heat treatment.

The results appeared to follow the inverse Hall–Petch effect [32]. Dislocations have been reported to play the primary role in the Hall–Petch effect, while in the inverse Hall–Petch effect, the film hardness is dominated by grain boundary sliding [32,33]. Consequently, the results of this study implied that the grain boundary structure is more relevant to the primary mechanical responses during indentation in SnO_2:F thin films. Decreasing the number of grain boundaries by increasing the grain size leads to the mechanical hardening of the film. In addition, the hardness and Young's modulus of polycrystalline materials are also significantly influenced by the presence of internal porosity. It has been reported that the Young's modulus of a material with a certain porosity is lower than that of its fully-dense counterpart [34,35]. In general, the Young's modulus decreases with increasing porosity, but this rate of increase slows down as the porosity increases further [36–38]. Deposition at higher flow rate of MBTC and the post-heat treatment increased densification (reduced porosity) due to the increased grain size and the improved film crystallinity. Therefore, these modifications improved the mechanical properties of the resulting films.

4. Conclusions

A range of FTO (SnO_2:F) thin films have been fabricated by atmosphere pressure chemical vapor deposition (APCVD) on an industrial production line. The structure and surface morphology of the FTO thin films were modified by increasing the flow rate of MBTC and by performing post-heat treatment. XRD analysis demonstrated enhanced crystallinity and preferential orientation along the (200) crystallographic plane in all polycrystalline FTO films. The roughness of the film surface morphology also increased from 14.5 nm to 29.4 nm. This phenomenon results from the formation of enlarged grains due to aggregation. As a consequence, both the Young's modulus and the hardness of FTO films were significantly improved due to the reduced grain boundaries and increased densification. The maximun values of the Young's modulus and hardness were ~235.9 GPa and ~15.89 GPa, respectively, which were observed for the post-heated FTO thin film prepared with the highest flow rate of MBTC, namely, 300 kg/h. This study has therefore paved the way for the industrial production of FTO thin films with advanced performance to support a wider range of future applications.

Acknowledgments

This work was financially supported by the National 'Twelfth Five-Year' Plan for Science & Technology Support (2011BAE14B02), the Ph.D. Programs Foundation of Ministry of Education of China (20100101120105), the National Natural Science Foundation of China (No. 51172200) and the Fundamental Research Funds for the Central University.

References

[1] K. Ellmer, Past achievements and future challenges in the development of optically transparent electrodes, Nature Photonics 6 (2012) 809–817.
[2] S. Mohammadi, H. Abdizadeh, M.R. Golobostanfard, Effect of niobium doping on opto-electronic properties of sol–gel based nanostructured indium tin oxide thin films, Ceramics International 39 (2013) 4391–4398.
[3] Q. Shi, K.S. Zhou, M.J. Dai, H.J. Hou, S.S. Lin, C.B. Wei, F. Hu, Room temperature preparation of high performance AZO films by MF sputtering, Ceramics International 39 (2013) 1135–1141.
[4] S.I. Noh, H.J. Ahn, D.H. Riu, Photovoltaic property dependence of dye-sensitized solar cells on sheet resistance of FTO substrate deposited via spray pyrolysis, Ceramics International 38 (2012) 3735–3739.
[5] H.M. Yates, P. Evans, D.W. Sheel, S. Nicolay, L. Ding, C. Ballif, The development of high performance SnO_2:F as TCOs for thin film silicon solar cells, Surface and Coatings Technology 213 (2012) 167–174.
[6] Z. Remes, M. Vanecek, H.M. Yates, P. Evans, D.W. Sheel, Optical properties of SnO_2:F films deposited by atmospheric pressure CVD, Thin Solid Films 517 (2009) 6287–6289.

[7] K.Y. Zeng, F.R. Zhu, J.Q. Hu, L. Shen, K.R. Zhang, H. Gong, Investigation of mechanical properties of transparent conducting oxide thin films, Thin Solid Films 443 (2003) 60–65.
[8] S.R. Jian, S.A. Ku, C.W. Luo, J.Y. Juang, Nanoindentation of GaSe thin films, Nanoscale Research Letters 7 (2012) 403.
[9] K.W. Chen, S.R. Jian, P.J. Wei, J.S.C. Jang, J.F. Lin, A study of the relationship between semi-circular shear bands and pop-ins induced by indentation in bulk metallic glasses, Intermetallics 18 (2010) 1572–1578.
[10] F. Atay, V. Bilgin, I. Akyuz, E. Ketenci, S. Kose, Optical characterization of SnO_2:F films by spectroscopic ellipsometry, Journal of Non-Crystalline Solids 356 (2010) 2192–2197.
[11] D.L. Guo, C.G. Hu, First-principles study on the electronic structure and optical properties for SnO_2 with oxygen vacancy, Applied Surface Science 258 (2012) 6987–6992.
[12] J.S. Jeng, The influence of annealing atmosphere on the material properties of sol–gel derived SnO_2:Sb films before and after annealing, Applied Surface Science 258 (2012) 5981–5986.
[13] H. Kaneko, K. Miyake, Physical properties of antimony-doped tin oxide thick films, Journal of Applied Physics 53 (1982) 3629–3633.
[14] Q. Gao, H. Jiang, C.J. Li, Y.P. Ma, X. Li, Z.H. Ren, Y. Liu, C.L. Song, G.R. Han, Tailoring of textured transparent conductive SnO_2:F thin films, Journal of Alloys and Compounds 574 (2013) 427–431.
[15] C. Agashe, J. Hüpkes, G. Schöpe, M. Berginski, Physical properties of highly oriented spray-deposited fluorine-doped tin dioxide films as transparent conductor, Solar Energy Materials and Solar Cells 93 (2009) 1256–1262.
[16] W.C. Oliver, G.M. Pharr, An improved technique for determining hardness and elastic modulus using load and displacement sensing indentation experiments, Journal of Materials Research 7 (1992) 1564–1583.
[17] A.C. Fischer-Cripps, Nanoindentation. Springer-Verlag, NewYork, 2002.
[18] H. Buckle, J.H. Westbrook, H. Conrad, The Science of Hardness Testing and Its Research Applications, ASTM, Philadelphia 263.
[19] A.F. Khan, M. Mehmood, M.A. Aslam, M. Ashraf, Characteristics of electron beam evaporated nanocrystalline SnO_2 thin films annealed in air, Applied Surface Science 256 (2010) 2252–2258.
[20] H.R. Fallah, M. Ghasemi, A. Hassanzadeh, H. Steki, The effect of annealing on structural, electrical and optical properties of nanostructured ITO films prepared by e-beam evaporation, Materials Research Bulletin 42 (2007) 487–496.
[21] C. Agashe, M. Takwale, V. Bhide, S. Mahamuni, S. Kulkarni, Effect of Sn incorporation on the growth mechanism of sprayed SnO_2 films, Journal of Applied Physics 70 (1991) 7382–7386.
[22] D. Belanger, J.P. Dodelet, B.A. Lombos, J.I. Dickson, Thickness dependence of transport properties of doped polycrystalline tin oxide films, Journal of the Electrochemical Society 132 (1985) 1398–1405.
[23] G. Gordillo, L.C. Moreno, W. de la Cruz, P. Teheran, Preparation and characterization of SnO_2 thin films deposited by spray pyrolysis from $SnCl_2$ and $SnCl_4$ precursors, Thin Solid Films 252 (1994) 61–66.
[24] Q. Gao, M. Li, X. Li, Y. Liu, C.L. Song, J.X. Wang, Q.Y. Liu, J.B. Liu, G.R. Han, Microstructural and functional stability of large-scale SnO_2:F thin film with micro-nano structure, Journal of Alloys and Compounds 550 (2013) 144–149.
[25] C.Y. Yen, S.R. Jian, G.J. Chen, C.M. Lin, H.Y. Lee, W.C. Ke, Y.Y. Liao, P.F. Yang, Y.S. Lai, J.S.C. Jang, J.Y. Juang, Influence of annealing temperature on the structural, optical and mechanical properties of ALD-derived ZnO thin films, Applied Surface Science 257 (2011) 7900–7905.
[26] C. Korber, J. Suffner, A. Klein, Surface energy controlled preferential orientation of thin films, Journal of Physics D: Applied Physics 43 (2010) 055301.
[27] W. Chen, H. Gong, K.Y. Zeng, Mechanical properties of Cu-Al-O thin films prepared by plasma-enhanced chemical vapor deposition, Journal of Vacuum Science and Technology A 24 (2006) 537–541.
[28] T.H. Fang, W.J. Chang, Nanomechanical characteristics of SnO_2:F thin films deposited by chemical vapor deposition, Applied Surface Science 252 (2005) 1863–1869.
[29] Y. Zhu, Y. Wang, P.F. Wan, H.Y. Li, S.Y. Wang, Optical and mechanical properties of transparent conductive Al-doped ZnO films deposited by the sputtering method, Chinese Physics Letters 29 (2012) 038103.
[30] G.A. Malygin, Plasticity and strength of micro- and nanocrystalline materials, Physics of the Solid State 49 (2007) 1013–1033.
[31] N. Kikuchi, E. Kusano, E. Kishio, A. Kinbara, Electrical and mechanical properties of SnO_2:Nb films for touch screens, Vacuum 66 (2002) 365–371.
[32] J. Schiotz, T. Vegge, F.D. Di Tolla, K.W. Jacobsen, Atomic-scale simulations of the mechanical deformation of nanocrystalline metals, Physical Review B 60 (1999) 11971–11983.
[33] H.V. Swygenhoven, Grain Boundaries and Dislocations, Science 296 (2002) 66–67.
[34] J. Chen, W. Wang, L.H. Qian, K. Lu, Critical shear stress for onset of plasticity in a nanocrystalline Cu determined by using nanoindentation, Scripta Materialia 49 (2003) 645–650.
[35] J. Luo, R. Stevens, Porosity-dependence of elastic moduli and hardness of 3Y-TZP ceramics, Ceramics International 25 (1999) 281–286.
[36] J. Musil, F. Kunc, H. Zeman, H. Polakova, Relationships between hardness, Young's modulus and elastic recovery in hard nanocomposite coatings, Surface and Coatings Technology 154 (2002) 304–313.
[37] J.B. Wachtman, Mechanical Properties of Ceramics, John Wiley and Sons, Inc, Canada, 1996.
[38] N. Ramakrishnan, V.S. Arunachalam, Effective elastic moduli of porous ceramic materials, Journal of the American Ceramic Society 76 (1993) 2745–2752.